Preparation of TiO$_2$-embedded carbon nanofibers and their photocatalytic activity in the oxidation of gaseous acetaldehyde

Soonhyun Kim *, Sang Kyoo Lim

Division of Nano-Bio Technology, Daegu Gyeongbuk Institute of Science and Technology (DGIST), Daegu 700-742, Republic of Korea

ARTICLE INFO

ABSTRACT

TiO$_2$-embedded carbon nanofibers (TiO$_2$/CNF) have been prepared by a simple method. TiO$_2$-embedded polyacrylonitrile fibers (TiO$_2$/PAN) were first prepared from a PAN solution containing TiO$_2$ particles by a simple electrospinning method, and subsequent carbonization and further oxidation of these led to TiO$_2$/CNF and oxidized TiO$_2$/CNF (Ox-TiO$_2$/CNF), respectively. Gaseous CH$_3$CHO was efficiently degraded with the concomitant production of CO$_2$ on the Ox-TiO$_2$/CNF composites under UV illumination. Although UV-illuminated TiO$_2$/PAN were also found to be capable of oxidizing gaseous CH$_3$CHO, these fibers underwent slow but spontaneous degradation. On the other hand, TiO$_2$/CNF had no effect on the photocatalytic oxidation of CH$_3$CHO, which may be attributed to the reduction and phase transformation of TiO$_2$ during carbonization. XPS results have shown that TiO$_2$ was partly reduced by carbonization and then re-oxidized during the further oxidation process. No anatase phase of TiO$_2$ was observed in the TiO$_2$/CNF composites, whereas this phase was unequivocally observed in the Ox-TiO$_2$/CNF composites. Moreover, the BET surface area was seen to be significantly enhanced by the further oxidation process, and this was responsible for the adsorption of CH$_3$CHO on the Ox-TiO$_2$/CNF. Therefore, the further oxidation process not only brings about re-oxidation of TiO$_2$ but also leads to a surface modification of the carbon nanofibers.

© 2008 Elsevier B.V. All rights reserved.

1. Introduction

TiO$_2$ photocatalysis has been extensively studied with regard to its application in environmental remediation processes [1–7]. The photocatalytic reactions are initiated by the absorption of UV photons with the concurrent generation of conduction band (CB) electrons and valence band (VB) holes in the TiO$_2$ lattice. The VB holes have strong oxidizing power and react with surface hydroxyl groups to produce $^\bullet$OH radicals. The remediation power of TiO$_2$ photocatalysts can be largely attributed to the strong oxidation potential of these $^\bullet$OH radicals. Recently, many researchers have been concerned with the photooxidation of volatile organic compounds (VOCs), which are emitted by numerous sources such as furniture and decoration materials, and which deserve attention due to their carcinogenicities [5–8].

For air purification, immobilized photocatalysts on support materials are usually employed [9–11]. Generally, surface area and activity are reduced by the immobilization of photocatalysts. Therefore, support materials with high surface areas have been applied to immobilize photocatalysts. For example, activated carbon has commonly been used as a support material [12–14]. Activated carbon has a high surface area, which is closely related to the enhancement of adsorption and photocatalytic activities. Another problem is insufficient adhesion between photocatalysts and support materials. To achieve good adhesion, complicated coating processes have been introduced. Therefore, it is necessary to search for simpler and more convenient immobilization methods. Some researchers have investigated the use of polymeric matrices as support materials. Iketani et al. recently prepared TiO$_2$/ poly(dimethylsiloxane) (PDMS) hybrid films on organic substrates from a TiO$_2$/PDMS hybrid sol [15]. Paschoalino et al. reported that orthophthalic polyester (OP)/TiO$_2$ films could be prepared from mixtures of OP polymer and TiO$_2$, and that the OP substrate showed resistance to degradation, good mechanical properties, and a useful lifetime after numerous applications [8]. On the other hand, some researchers have recently reported that carbon nanofibers may be prepared from polyacrylonitrile (PAN) solutions by electrospinning methods [16–18]. Electrospinning technology offers a simple method for making ultra-thin fibers from various polymer solutions [19]. It has also been extended to the fabrication of inorganic/organic hybrid nanofibers [20,21]. Moreover, nanoparticles can be directly added to the solution used for
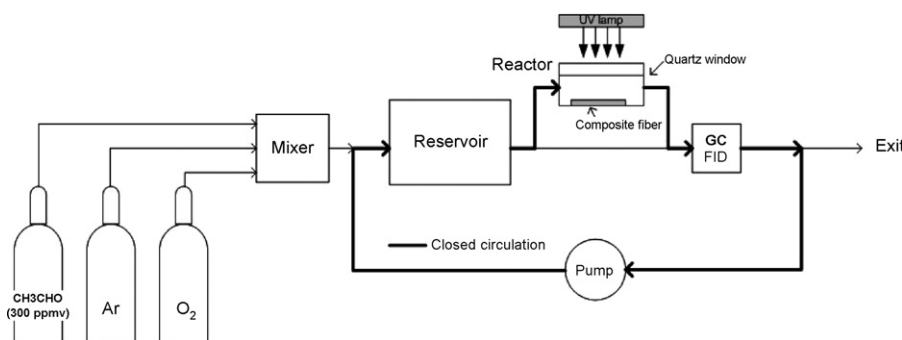
Fig. 1. Schematic of the experimental set-up for the photocatalytic oxidation of gaseous CH_3CHO.

electrospinning in order to obtain nanofibers. Therefore, using these electrospinning techniques, photocatalysts may be easily embedded into carbon nanofibers.

In this work, we have prepared TiO_2-embedded PAN fibers (TiO_2/PAN) from PAN solutions containing TiO_2 particles by an electrospinning method. Subsequent calcination of the TiO_2/PAN under an N_2 atmosphere produced TiO_2-embedded carbon nanofibers (TiO_2/CNF). Finally, thermal treatment of the TiO_2/CNF under oxidative conditions resulted in oxidized TiO_2/CNF (Ox-TiO_2/CNF). The physicochemical properties of these composites have been measured and their photocatalytic activities in the oxidation of CH_3CHO have been investigated. The relationships between their physicochemical properties and photocatalytic activities are discussed.

2. Experimental

2.1. Preparation of composite fibers

PAN and N,N-dimethylformamide (DMF) were purchased from Aldrich and Samchun, respectively. These reagents were used as received. Commercial TiO_2 (Hombikat UV 100) was used as the photocatalyst. A 10 wt.% solution of PAN in DMF was prepared by stirring the polymer and solvent at 45 °C for 20–30 h so as to obtain a homogeneous solution. TiO_2 was dispersed in this PAN/DMF solution by stirring and the mixture was sonicated in order to ensure good dispersal. In this way, a yellowish viscous PAN/TiO_2 gel was prepared.

The TiO_2/PAN were fabricated by an electrospinning method according to the literature [16–19,22,23]. The viscous PAN/TiO_2 gel was placed in a hypodermic syringe, which was positioned at a fixed distance (12 cm) from a metal cathode (collector). Dense webs of nanofibers were collected under an applied potential of 20 kV. For the preparation of TiO_2/CNF, the TiO_2/PAN were placed in a tube furnace, stabilized in air for 30 min at 250 °C, then carbonized for 1 h at 750 °C, and finally heated at 1000 °C in an N_2 atmosphere for a further 1 h. The ramp rate was 5 °C/min between the 250, 750, and 1000 °C plateaus. TiO_2/CNF was calcined for 3 h at 400 °C in air, which resulted in its oxidation to Ox-TiO_2/CNF. For comparison, we also prepared PAN nanofibers, carbon nanofibers (CNF), and oxidized CNF (Ox-CNF).

2.2. Photocatalysis and characterization of the composite fibers

The experimental set-up for the photocatalytic oxidation of CH_3CHO is illustrated schematically in Fig. 1. The photocatalytic oxidation of CH_3CHO was carried out in a closed-circulation reactor under ambient conditions as described elsewhere [4,5]. Gases used were CH_3CHO (300 ppmv in N_2) as a CH_3CHO standard, O_2 (99.9999%), and Ar (99.9999%) as carrier gas. The concentration of

CH_3CHO was 15–20 ppmv. Firstly, the mixed gas passed through the reservoir (volume 600 cm^3) and the concentration of CH_3CHO in the exit stream was monitored until it attained a constant value; the gas was then circulated by means of the pump. Next, the circulated gas was passed through a stainless steel reactor (volume 20 cm^3) with a quartz window so that it came into contact with the surface of a composite placed in a stainless steel reactor. After an adsorption equilibrium with the surface of the composite had been established in the dark, the catalyst was illuminated with UV light. All composite fiber samples weighed about 4–5.5 mg and were in the form of rectangular mats of dimensions 3 cm × 2.5 cm. The reactor was placed in a wooden box (40 cm × 40 cm × 50 cm) that housed a 250 W Hg lamp. The distance between the sample and the lamp was 15 cm. The removal of CH_3CHO and the production of CO_2 were monitored using a gas chromatograph (GC, HP6890) that was equipped with a Porapak-Q column, a flame ionization detector (FID), a CO_2 methanizer (Ni catalyst), and a gas-sampling valve.

The surface morphological images of the composite fibers were obtained by using a field emission scanning electron microscope (FE-SEM, Hitachi S-4200). The carbon and nitrogen contents were measured with an elemental analyzer (LECO CHNS932). XRD patterns were obtained with an X-ray diffractometer (Rigaku D/MAX-2500, 18 kV) using Cu $K\alpha_1$ radiation. BET surface area measurements were carried out by using N_2 as the adsorptive gas. The oxidation states of the Ti atoms were determined by X-ray photoelectron spectroscopy (XPS) (Kratos XSAM 800pci) using the Mg $K\alpha$ line (1253.6 eV) as the excitation source.

3. Results and discussion

3.1. TiO_2-embedded carbon fibers

Fig. 2 shows SEM images of TiO_2/PAN, TiO_2/CNF, and Ox-TiO_2/CNF. It can clearly be seen that the TiO_2 particles are randomly embedded in the fibers. After the carbonization process, the diameter of the fibers was seen to be decreased, due to weight loss through carbonization and densification at elevated temperatures [21]. The morphology of the TiO_2/CNF was not significantly changed by the post-oxidation process.

However, after post-oxidation, the total carbon and nitrogen contents were significantly reduced and the BET surface areas of the composite fibers were increased from 35 to 604 m^2/g and from 42 to 223 m^2/g for CNF and TiO_2/CNF, respectively, as shown in Tables 1 and 2. These results indicate that the carbon fibers were thermally activated during the post-oxidation process. Generally, for the activation of carbon materials, an activating agent such as KOH is used [24]. Although no activating agent was present in our system, the carbon in the CNF was able to react with oxygen and subsequently some carbon atoms were seemingly released in gaseous form.
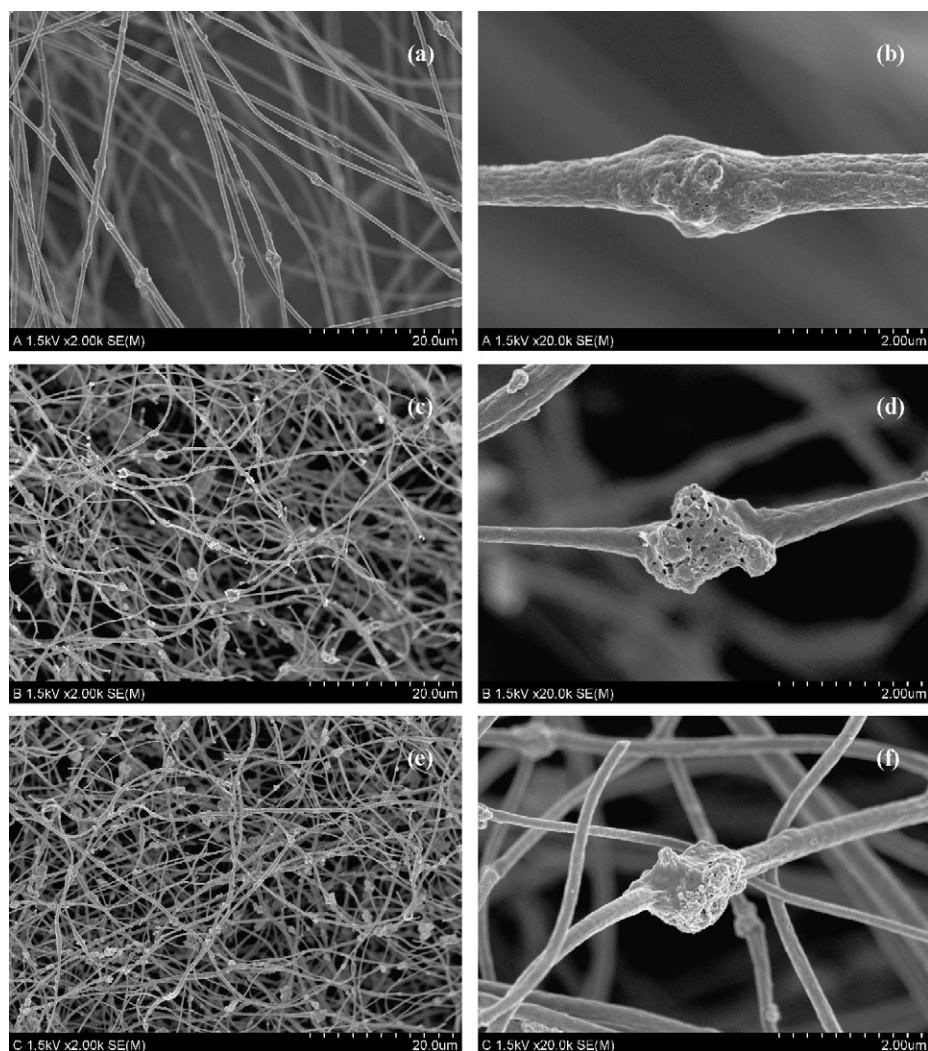
Fig. 2. SEM images of TiO_2-embedded composite fibers: (a and b) TiO_2/PAN, (c and d) TiO_2/CNF, and (e and f) Ox-TiO_2/CNF.

Fig. 3 shows the X-ray diffraction patterns of TiO_2/PAN, TiO_2/CNF, and Ox-TiO_2/CNF. Typically, such nanofibers exhibit an equatorial peak [17,25]. In this work, the equatorial peak of PAN fibers was observed in TiO_2/PAN at $2\theta = 16.7°$ and then disappeared upon carbonization and post-oxidation. The peaks of crystalline TiO_2 were also apparent. For TiO_2/PAN, the anatase peak was unambiguously observed, since commercial TiO_2 (Hombikat UV 100) is entirely composed of the anatase phase. After carboniza-

tion, almost all of the anatase phase had disappeared (Fig. 3b) or had been transformed to the rutile phase (Fig. 3c). Generally, rutile is more stable than anatase at high temperatures, and hence the phase transformation from anatase to rutile occurs upon heating

Table 1
Carbon and nitrogen contents (%)

Content	TiO_2-embedded fibers			Fibers only		
	C	N	C + N	C	N	C + N
Electrospinning	54.44	23.94	78.38	65.93	29.63	95.56
Carbonization	63.99	7.49	71.48	86.25	7.28	93.53
Post-oxidation	45.44	5.39	50.83	71.17	7.57	78.74

Table 2
BET surface areas (m^2/g)

	TiO_2-embedded fibers	Fibers only
Carbonization	42 ± 2.98	35 ± 4.13
Post-oxidation	223 ± 4.63	604 ± 18.74
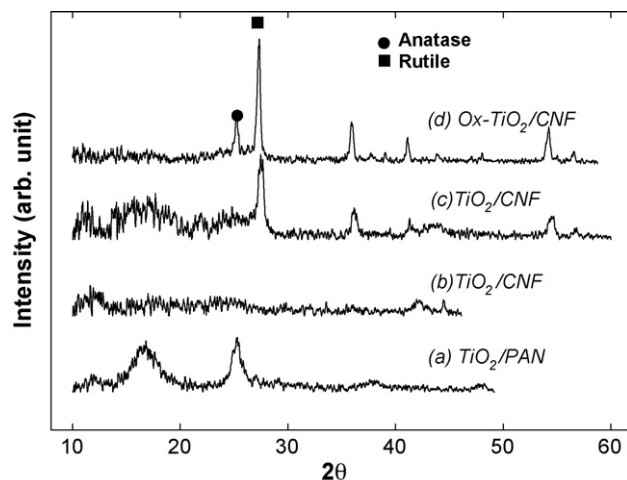
Fig. 3. XRD patterns of TiO_2-embedded composite fibers: (a) TiO_2/PAN, (b and c) TiO_2/CNF, (d) Ox-TiO_2/CNF.
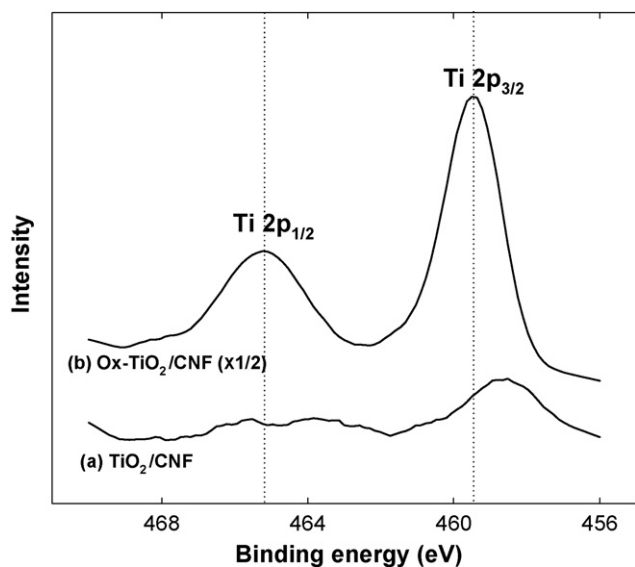
Fig. 4. XPS spectra of (a) TiO$_2$/CNF and (b) Ox-TiO$_2$/CNF composites in the Ti 2p band region.

[26], as was the case in the present carbonization process. A part of the TiO$_2$ seems to be reduced during carbonization under an N$_2$ atmosphere, which might be attributed to a carbothermal reduction process. This reaction may be described as follows Eq. (1) [27,28]:

$$TiO_{2solid} + carbon_{solid}[+nitrogen_{gas}] \rightarrow Ti(CO[N])_{solid} + CO_{gas} \qquad (1)$$

Interestingly, the anatase phase was seen to have reappeared in Ox-TiO$_2$/CNF, which implies that the reduced TiO$_2$ was oxidized by the thermal treatment in air. This result might be closely related to the photocatalytic degradation of CH$_3$CHO.

The oxidation state of the Ti was monitored by XPS analysis. Fig. 4 compares the Ti 2p bands in the XPS spectra of TiO$_2$/CNF and Ox-TiO$_2$/CNF. The Ti 2p$_{1/2}$ and Ti 2p$_{3/2}$ signals for Ox-TiO$_2$/CNF are seen to be located at binding energies of 465.21 and 459.46 eV, respectively. This is in agreement with the reported literature values for TiO$_2$ [29,30]. However, the Ti 2p signals for TiO$_2$/CNF are seen to be shifted to lower binding energies which indicates the presence of reduced Ti states. Bullen and Garrett reported that the Ti 2p$_{3/2}$ peaks in TiO$_2$, Ti$_2$O$_3$, and TiO are located at binding energies of 459.0, 457.6, and 455.3 eV, respectively. Therefore, the valence state of Ti in TiO$_2$/CNF might comprise a mixture of Ti(IV) and Ti(III) states. This result supports the view that the TiO$_2$ embedded in the carbon fibers was partly reduced during the carbonization and then re-oxidized during the post-oxidation process in air. Generally, the reduced titanium phases, such as the black Ti$_2$O$_3$, exhibited lower photocatalytic activities relative to the anatase TiO$_2$ [31]. From these observations, we could expect that the photocatalytic activities of Ox-TiO$_2$/CNF might be higher than that of TiO$_2$/CNF.

3.2. Photocatalytic oxidation of acetaldehyde

Fig. 5 shows the removal of CH$_3$CHO and the production of CO$_2$ by the UV-illuminated composite fibers. Before UV irradiation, CH$_3$CHO was pre-contacted with the sample for 30 min. Direct photolytic degradation of CH$_3$CHO was not observed at all. With PAN nanofibers or TiO$_2$/PAN (Fig. 5a), there was no adsorption of CH$_3$CHO upon contact with these composites. CH$_3$CHO was not degraded by UV-illuminated PAN nanofibers, and PAN nanofibers themselves were not degraded by UV illumination. However, with
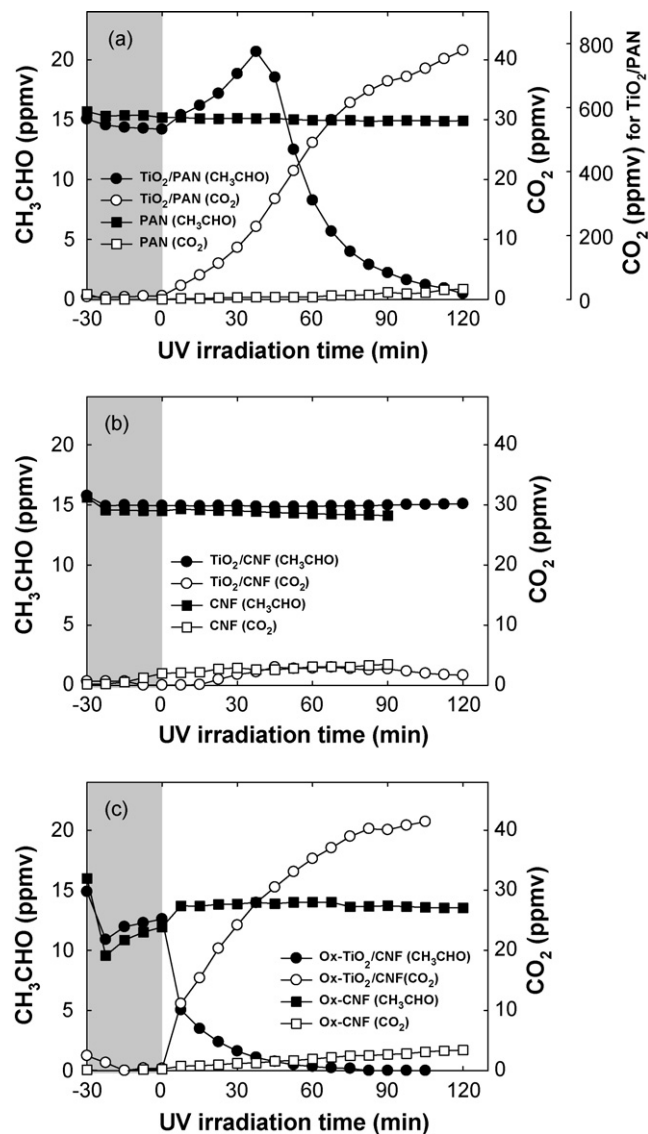
Fig. 5. Photocatalytic degradation of CH$_3$CHO and production of CO$_2$ on composite fibers: (a) electrospun, (b) carbonized, and (c) post-oxidized. Before irradiation, CH$_3$CHO was in contact with the composite fibers for 30 min (dark gray shading). The different concentrations of CH$_3$CHO before irradiation may be attributed to its adsorption on the composite fibers.
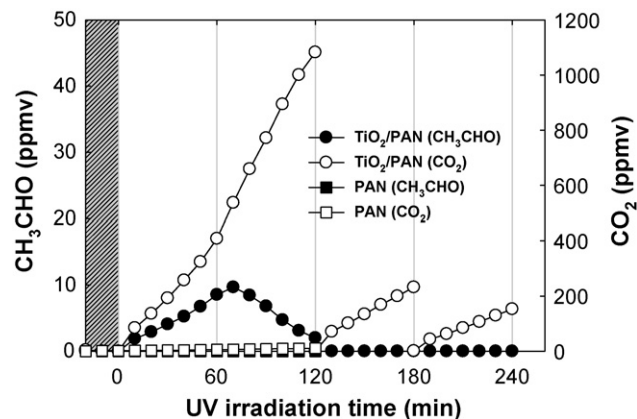
Fig. 6. Photocatalytic production of CH$_3$CHO and CO$_2$ on UV-illuminated electrospun composite fibers. After 120 min of irradiation, CO$_2$ in the reactor was flushed out by a flow of Ar/O$_2$ and UV-irradiation was continued for 60 min. This procedure was repeated.

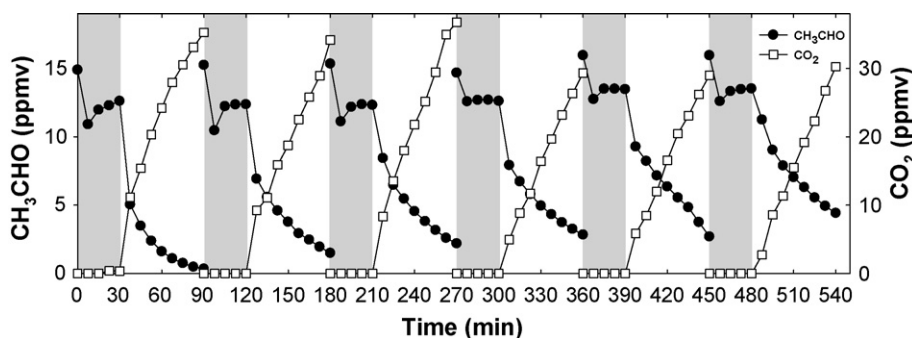**Fig. 7.** Repeated runs of the photocatalytic oxidation of CH_3CHO on Ox-TiO_2/CNF.

TiO_2/PAN, the concentration of CH_3CHO initially increased and then drastically decreased with the concomitant production of a significant amount of CO_2. This result can be attributed to the photocatalytic production of CH_3CHO from PAN nanofibers or degradation of residual DMF solvent by the TiO_2 photocatalyst as shown in Fig. 6. Fig. 6 shows the production of CH_3CHO and CO_2 from UV-illuminated TiO_2/PAN in the absence of CH_3CHO.

With CNF or TiO_2/CNF produced from the carbonization of PAN nanofibers or TiO_2/PAN, the concentration of CH_3CHO did not decrease at all and CO_2 production was negligible, as shown in Fig. 5b. This result indicates that there is neither adsorption nor degradation of gaseous CH_3CHO on CNF or TiO_2/CNF.

However, subjecting CNF and TiO_2/CNF to a post-oxidation process strongly changed their activities in the adsorption and photooxidation of CH_3CHO. Fig. 5c shows that CH_3CHO was adsorbed on both the Ox-CNF and Ox-TiO_2/CNF and was efficiently oxidized by UV-illuminated Ox-TiO_2/CNF. The adsorption of CH_3CHO seems to be closely related to the surface areas of the composites (Table 2). The increased surface area resulting from the post-oxidation process is thus likely to be responsible for the more effective adsorption of CH_3CHO on the surfaces of the Ox-CNF and Ox-TiO_2/CNF composites. Photocatalytic oxidation of CH_3CHO with the concomitant production of CO_2 occurred efficiently on the Ox-TiO_2/CNF, which was due to the anatase phase of TiO_2 as shown in Fig. 3. On the other hand, desorption of CH_3CHO adsorbed on Ox-CNF was observed immediately after UV irradiation, suggesting photo-induced desorption. Kim and Choi [5] have also observed the photo-induced desorption of CH_3CHO adsorbed on TiO_2.

To investigate whether or not Ox-TiO_2/CNF becomes deactivated, the photocatalytic oxidation of CH_3CHO was repeated over six cycles, as shown in Fig. 7. The photocatalytic oxidation of CH_3CHO with the concomitant production of CO_2 slowly decreased during the repeat cycles. This result indicates that TiO_2-embedded carbon nanofibers are slowly deactivated and hence further modifications of this composite fiber are needed to prevent deactivation.

4. Conclusions

We have prepared TiO_2-embedded carbon nanofibers. TiO_2/PAN composite nanofibers were prepared by a simple electro-spinning method from a PAN solution containing TiO_2 particles, and through subsequent carbonization and post-oxidation procedures these composites were converted into TiO_2/CNF and Ox-TiO_2/CNF composites, respectively. The post-oxidized Ox-TiO_2/CNF composites showed efficient activities in the photocatalytic oxidation of CH_3CHO with the concomitant production of

CO_2 under UV irradiation. TiO_2 embedded in the composite fibers was partly reduced during carbonization and then re-oxidized in the post-oxidation process. The oxidized TiO_2 in the carbon nanofiber composites is considered to be responsible for the photocatalytic oxidation of CH_3CHO under UV irradiation. Moreover, the BET surface area of the composite fibers was enhanced by the post-oxidation, allowing the adsorption of gaseous CH_3CHO.

References

[1] M.R. Hoffmann, S.T. Martin, W. Choi, D.W. Bahnemann, Chem. Rev. 95 (1995) 69–96.
[2] S. Kim, W. Choi, Environ. Sci. Technol. 36 (2002) 2019–2025.
[3] H. Lee, W. Choi, Environ. Sci. Technol. 36 (2002) 3872–3878.
[4] S. Hwang, M.C. Lee, W. Choi, Appl. Catal. B: Env. 46 (2003) 49–63.
[5] H. Kim, W. Choi, Appl. Catal. B: Env. 69 (2006) 127–132.
[6] Y. Ohko, D.A. Tryk, K. Hashimoto, A. Fujishima, J. Phys. Chem. B 102 (1998) 2699–2704.
[7] H. Einaga, S. Futamura, T. Ibusuki, Appl. Catal. B: Env. 38 (2002) 215–225.
[8] M.P. Paschoalino, J. Kiwi, W.F. Jardim, Appl. Catal. B: Env. 68 (2006) 68–73.
[9] R.M. Alberici, W.F. Jardim, Appl. Catal. B: Env. 14 (1997) 55–68.
[10] M.L. Sauer, D.F. Ollis, J. Catal. 149 (1994) 81–91.
[11] W. Choi, J.Y. Ko, H. Park, J.S. Chung, Appl. Catal. B: Env. 31 (2001) 209–220.
[12] T. Torimoto, S. Ito, S. Kuwabata, H. Yoneyama, Environ. Sci. Technol. 30 (1996) 1275–1281.
[13] X. Zhang, M. Zhou, L. Lei, Carbon 43 (2005) 1700–1708.
[14] B. Herbig, P. Lobmann, J. Photochem. Photobiol. A: Chem. 163 (2004) 359–365.
[15] K. Iketani, R.-D. Sun, M. Toki, K. Hirota, O. Yamaguchi, J. Phys. Chem. Solids 64 (2003) 507–513.
[16] S.Y. Gu, J. Ren, Q.L. Wu, Synt. Met. 155 (2005) 157–161.
[17] E. Zussman, X. Chen, W. Ding, L. Calabri, D.A. Dikin, J.P. Quintana, R.S. Ruoff, Carbon 43 (2005) 2175–2185.
[18] S. Wang, Z.-H. Chen, W.-J. Ma, Q.-S. Ma, Ceram. Int. 32 (2006) 291–295.
[19] D. Li, Y. Xia, Adv. Mater. 16 (2004) 1151–1170.
[20] Q.B. Yang, D.M. Li, Y.L. Hong, Z.Y. Li, C. Wang, S.L. Qiu, Y. Wei, Synt. Met. 137 (2003) 973–974.
[21] Y. Yang, H. Wang, X. Lu, Y. Zhao, X. Li, C. Wang, Mater. Sci. Eng. B 140 (2007) 48–52.
[22] C.-H. He, J. Gong, Polm. Degrad. Stab. 81 (2003) 117–124.
[23] S.K. Lim, S.-K. Lee, S.-h. Hwang, H. Kim, Macromol. Mater. Eng. 291 (2006) 1265–1270.
[24] Q. Jiang, Y. Zhao, Microporous Mesoporous Mater. 76 (2004) 215–219.
[25] X.D. Liu, W. Ruland, Macromolecules 26 (1993) 3030–3036.
[26] X. Ye, J. Sha, Z. Jiao, L. Zhang, Nanostruct. Mater. 8 (1997) 919–927.
[27] L.-M. Berger, W. Gruner, E. Langholf, S. Stolle, Int. J. Refract. Met. Hard Mater. 17 (1999) 235–243.
[28] L.-M. Berger, W. Gruner, Int. J. Refract. Met. Hard Mater. 20 (2002) 235–251.
[29] B. Erdem, R.A. Hunsicker, G.W. Simmons, E.D. Sudol, V.L. Dimonie, M.S. El-Aaser, Langmuir 17 (2001) 2664–2669.
[30] H.A. Bullen, S.J. Garrett, Nano Lett. 2 (2002) 739–745.
[31] S. Perera, N. Zelenski, E.G. Gillan, Chem. Mater. 18 (2006) 2381–2388.